Catalysis Today 165 (2011) 41–48

Contents lists available at ScienceDirect

Catalysis Today

journal homepage: www.elsevier.com/locate/cattod

Reactivity of hydrogen and methanol on (0 0 1) surfaces of WO_3, ReO_3, WO_3/ReO_3 and ReO_3/WO_3

Sanliang Ling[a,*], Donghai Mei[b], Maciej Gutowski[a]

[a] Chemistry-School of Engineering and Physical Sciences, Heriot-Watt University, Edinburgh EH14 4AS, UK
[b] Institute for Interfacial Catalysis, Pacific Northwest National Laboratory, Richland, WA 99352, USA

ARTICLE INFO

Article history:
Received 20 October 2010
Received in revised form
14 December 2010
Accepted 9 January 2011
Available online 12 February 2011

Keywords:
Tungsten trioxide
Rhenium trioxide
Heterostructure
Epitaxy
Methanol
Hydrogen
Density functional theory

ABSTRACT

Bulk tungsten trioxide (WO_3) and rhenium trioxide (ReO_3) share very similar structures but display different electronic properties. WO_3 is a wide bandgap semiconductor while ReO_3 is an electronic conductor. With the advanced molecular beam epitaxy techniques, it is possible to make heterostructures comprised of layers of WO_3 and ReO_3. These heterostructures might display reactivity different than pure WO_3 and ReO_3. The interactions of two probe molecules (hydrogen and methanol) with the (0 0 1) surfaces of WO_3, ReO_3, and two heterostructures ReO_3/WO_3 and WO_3/ReO_3 were investigated at the density functional theory level. Atomic hydrogen prefers to adsorb at the mono-coordinated O (O_{1C}) sites forming a surface hydroxyl on four surfaces. Dissociative adsorption of a hydrogen molecule at the O_{1C} site leads to formation of a water molecule adsorbed at the penta-coordinated metal (M_{5C}) site. This is thermodynamically the most stable state. A thermodynamically less stable dissociative state involves two surface hydroxyl groups $O_{1C}H$ and $O_{2C}H$. The interaction of molecular hydrogen and methanol with pure ReO_3 is stronger than with pure WO_3 and the strength of the interaction substantially changes on the WO_3/ReO_3 and ReO_3/WO_3 heterostructures. The reaction barriers for decomposition and recombination reactions are sensitive to the nature of heterostructure. The calculated adsorption energy of methanol on WO_3(0 0 1) of −65.6 kJ/mol is consistent with the previous experimental estimation of −67 kJ/mol.

1. Introduction

Metal oxides have been widely used as both catalysts and support materials in heterogeneous catalysis. Generally, insulating metal oxides show limited catalytic activity while conductive metal oxides show high activity with respect to some of heterogeneous reactions such as selective oxidation of alcohols [1–6]. With recent advances in molecular beam epitaxy technology, new types of "heterostructure" or "heterojunction" materials became available [7]. These heterostructures of metal oxides that are built from layers of structurally similar but electronically different transition metal oxides could be used as new catalysts with tunable activity and selectivity. For example, an epitaxial interface between α-Fe_2O_3 and α-Cr_2O_3 showed non-commutative properties and photocatalytic applications were suggested [8]. Further theoretical study unraveled that the α-Fe_2O_3/α-Cr_2O_3 and α-Cr_2O_3/α-Fe_2O_3 heterostructures have different interfaces. This difference is responsible for non-commutative band offsets and magnetic properties of the interface [9]. Further chemical modifications of the interface were suggested to control the magnitude of band offsets [10]. Tungsten trioxide (WO_3) has a band gap of 2.6 eV [11] while rhenium trioxide (ReO_3) is conductive. Interestingly, monoclinic WO_3 and cubic ReO_3 have commensurate lattice parameters. Thus, heterostructures constructed from WO_3 and ReO_3 may show unique reactivity due to the combination of oxides with different electronic structures.

Supported WO_3 is catalytically active for the dehydration of alcohols [4,5,12,13]. Tanner et al. studied the dehydration of a series of alcohols on the monoclinic γ-WO_3(0 0 1) surface using scanning tunneling microscopy and temperature-programmed desorption [13]. They found the penta-coordinated metal sites on the WO_3(0 0 1) surface are responsible for the oxidative dehydration. No dehydrogenation of alcohols was observed. As the temperature increases, alcohols convert into alkoxides, and then desorb as alkenes. Water molecule is formed by deprotonation of surface hydroxyls [12]. Ma et al. studied the reactivities of ethanol and 2-propanol on the fully oxidized and reduced WO_3(0 0 1) surfaces [5]. Their results suggested that both ethanol and 2-proponal molecules are stable until 450 K. Upon further temperature increase, the alkoxy intermediates (dehydrated from alcohols) decompose into alkenes. Methanol only dissociates on the reduced WO_3(0 0 1) surface [4]. The reduced WO_3(0 0 1) surface shows a slightly higher activity, but does not substantially change

* Corresponding author.
E-mail addresses: s.ling@hw.ac.uk (S. Ling), donghai.mei@pnl.gov (D. Mei), m.gutowski@hw.ac.uk (M. Gutowski).

0920-5861/$ – see front matter © 2011 Elsevier B.V. All rights reserved.
doi:10.1016/j.cattod.2011.01.017

reaction paths. On the contrary, alcohol dehydrogenation occurs on the supported ReO_3 catalysts. A high activity was found for selective methanol oxidation to methylal on V_2O_5-, ZrO_2-, Fe_2O_3- and TiO_2-supported ReO_3 [6,14]. Adsorbed methanol first dehydrogenates into formaldehyde (CH_2O), which could react with lattice oxygen of ReO_3 forming dioxymethylene (–H_2COO). Methylal is produced by oxidative coupling of dioxymethylene with neighboring methoxy (CH_3O) or methanol [2]. The reactivity of methanol on heterostructures of WO_3 and ReO_3 will be explored in the current study.

A number of previous studies indicated that non-stoichiometric hydrogen bronze H_xWO_3/H_xReO_3 ($0.1 < x < 0.5$) phases are formed from WO_3 and ReO_3 exposed to hydrogen [15,16]. Adsorption of hydrogen molecules on WO_3 could also lead to metallic tungsten trioxide via formation of hydroxyl groups and desorption of water [17]. As such, after hydrogen adsorbs on WO_3 or ReO_3, it will either migrate into the bulk structure forming hydrogen bronze or recombine to form water on the surface. Herein we only focus on the interaction of hydrogen with (0 0 1) surfaces of WO_3 or ReO_3, and their heterostructures.

Since the W^{6+} 5d band is empty while the Re^{6+} has $5d^1$ electronic configuration, the bulk WO_3 has a band gap of 2.6 eV [11] while ReO_3 is an electronic conductor. The crystalline and electronic structures of ReO_3 and WO_3 have been investigated using density functional theory (DFT) calculations [3,18,19]. In agreement with experimental measurements [20,21], Cora et al. found that ReO_3 is cubic while WO_3 has a distorted cubic structure with off-center displacements of metal ions [3]. The monoclinic structure of WO_3 results from covalent interactions between the metal ion and the nearest oxygen atoms while the presence of the antibonding levels in the conduction band of ReO_3 opposes structural deformations. Yakovkin and Gutowski studied the WO_3(0 0 1) surfaces with various types of terminations [18]. They found that the redistribution of density of states near the Fermi level leads to a dramatic decrease of surface electron energy. Consequently, a noticeable distortion and tilting of the surface W atoms were observed in the relaxed surface structure. They also found that the non-polar $c(2 \times 2)$ O-terminated WO_3(0 0 1) slab is more stable than the polar slab with the (1×1) WO_2-termination on one side and the (1×1) O-termination on the other side of the slab [18]. Ge and Gutowski calculated adsorption of methanol on the (0 0 1) surfaces of WO_3 and ReO_3. The surface of ReO_3 proved to be much more reactive and favored dissociation of methanol and formation of a methoxy group. The difference in reactivity between the surfaces of WO_3 and ReO_3 was attributed to the partially occupied conduction band of ReO_3, the orbitals of which interact with the orbitals of the hydroxyl group of methanol [19].

Here we study whether heterostructures made of non-conductive WO_3 and conductive ReO_3 display different reactivity than slabs of pure ReO_3 and WO_3. Two simple molecules, i.e., hydrogen and methanol, are used as probes to test the reactivity. The non-polar $c(2 \times 2)$ O-terminated (0 0 1) orientation was chosen for all four surfaces. The ReO_3/WO_3 heterostructure is constructed by replacing the top layer of WO_3(0 0 1) with a ReO_3 overlayer. Similarly, the WO_3/ReO_3 heterostructure is constructed with one WO_3 layer on top of ReO_3(0 0 1). The effects of heterostructures on binding energies and reaction barriers were studied at the DFT level of theory.

2. Computational details

The periodic DFT calculations were performed with the Vienna Ab initio Simulation Package (VASP) [22,23] using a plane wave basis set with a cutoff energy of 400 eV. The Perdew–Burke–Ernzerhof (PBE) functional [24] with the projector augmented wave (PAW) method [25,26] was used to solve the Kohn–Sham equations for crystalline slabs. A Gaussian type of electronic smearing with a width of 0.1 eV was used to improve convergence of electronic self-consistent field calculations. The ground state geometry optimizations of bulk and surfaces were considered converged if the maximum force on relaxed atoms falls below 0.01 eV/Å. Spin-polarization was needed to describe adsorption of atomic hydrogen. For bulk structure calculations, Monkhorst–Pack k-point grids [27] of $(9 \times 9 \times 9)$ and $(5 \times 5 \times 3)$ were used for ReO_3 and WO_3, respectively. The optimized lattice constant of 3.764 Å for the perfect cubic ReO_3 structure is in good agreement with the experimental value of 3.748 Å [21]. The optimized lattice parameters of bulk monoclinic WO_3, $a = 5.252$ Å, $b = 5.043$ Å, $c = 7.550$ Å and $\beta = 93.210^\circ$, are also in good agreement with the experimental values of $a = 5.278$ Å, $b = 5.156$ Å, $c = 7.664$ Å and $\beta = 91.762^\circ$ [20].

The (0 0 1) surface slab with a $c(2 \times 2)$ super cell of ReO_3 and WO_3 were constructed from the optimized bulk structures, see Fig. 1. The two heterostructure, WO_3/ReO_3 and ReO_3/WO_3, were modeled by replacing the top layer with another oxide, see Fig. 1. Only minor slab relaxation was found for two heterostructures in the course of geometry optimization. A vacuum layer of 15.0 Å was inserted in the z direction to avoid unphysical interactions between adjacent slabs. The adsorbed molecule as well as the atoms in the two top layers of the slab is allowed to relax while the atoms in the bottom two layers are fixed. Different k-point grids were tested and a $(3 \times 3 \times 1)$ k-point sampling was found accurate enough for surface calculations. For density of states (DOS) calculations, k-point grids of $(5 \times 5 \times 1)$ were used. The Bader's charge analysis [28] was performed using the method developed by Henkelman et al. [29]. All geometry optimizations were performed by using a conjugate-gradient or quasi-Newton schemes as implemented in VASP. The adsorption energy of H, H_2, and CH_3OH is calculated as follows:

$$E_{ads} = E_{adsorbate+surface} - (E_{surface} + E_{adsobate}) \quad (1)$$

where $E_{adsorbate+surface}$ is the total energy of the adsorbate interacting with the surface slab; $E_{surface}$ is the total energy of the optimized surface slab; $E_{adsorbate}$ is the energy of a single hydrogen atom, a hydrogen molecule or a methanol molecule in vacuum. A negative E_{ads} value indicates the adsorption is energetically favorable.

Transition states were located using the climbing image nudged elastic band (CI-NEB) method [30]. The reaction energy is calculated as the energy difference between the final state and the initial state. The forward and reverse activation barriers of each reaction path are defined as the energy difference between the transition state and the initial and final state, respectively.

3. Results and discussion

3.1. Layered WO_3/ReO_3 structures

Here we discuss the stability and properties of layered ReO_3/WO_3 structures. The surface energy is lower for WO_3(0 0 1) than for ReO_3(0 0 1), 1.9×10^{-2} eV/Å^2 vs 5.3×10^{-2} eV/Å^2 [18] because the monoclinic structure is more suitable for surface relaxation than the cubic structure. We explored the relative energy of hypothetical bulk $WReO_6$ structures, with eight metal atoms per unit cell, as a function of distribution of metal atoms, see Fig. 2a–c. The energies were referenced with respect to the sum of properly weighted energies of bulk WO_3 and ReO_3. It is remarkable that the (0 0 1) heterostructure, structure c in Fig. 2, is more stable than the structures a and b by 0.09 and 0.21 eV, respectively, and barely unstable with respect to the bulk WO_3 and ReO_3. In other words, the layered (0 0 1) heterostructures do not favor mixing of W and Re in the (0 0 1) planes. This result supports our selection of WO_3/ReO_3 and ReO_3/WO_3 (0 0 1) heterostructures for evaluation of their reactivity with hydrogen and methanol. One should

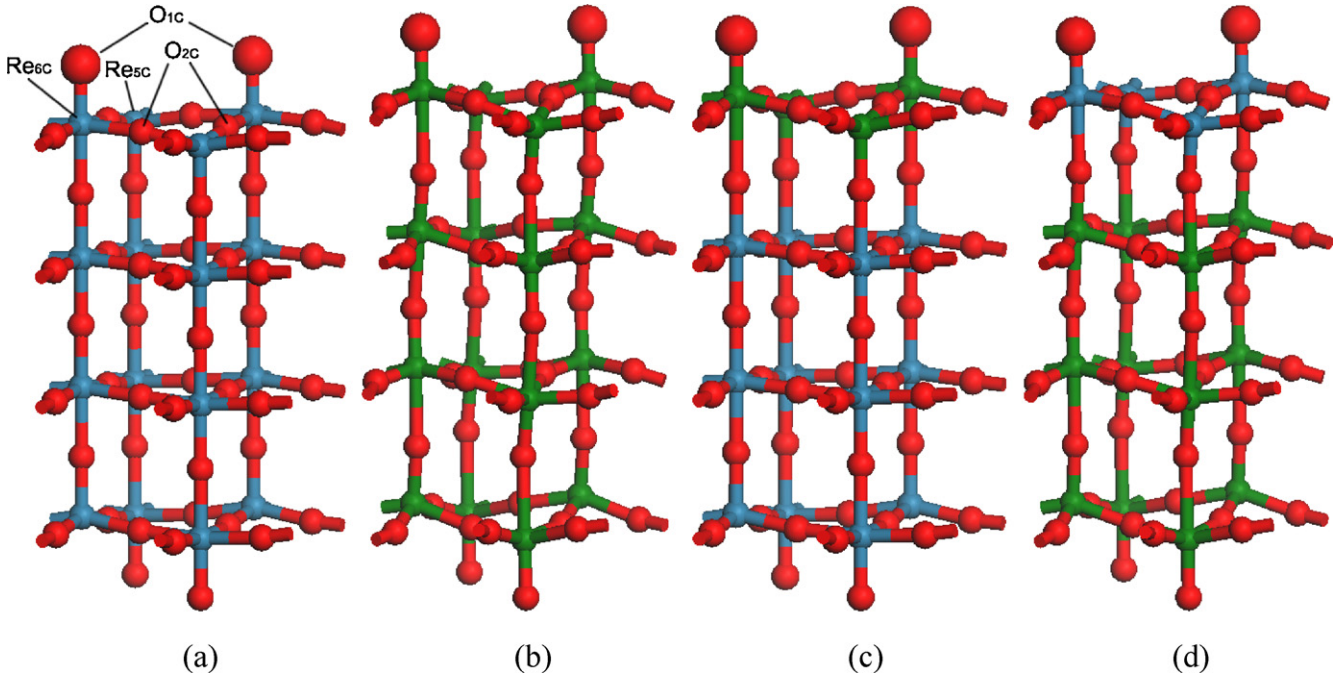

Fig. 1. Side views of the optimized clean (0 0 1) surface structures of (a) ReO_3; (b) WO_3; (c) WO_3/ReO_3; (d) ReO_3/WO_3. Oxygen atoms are in red; rhenium atoms are in blue; tungsten atoms are in green.

keep in mind that epitaxial heterostructures are frequently stable kinetically rather than thermodynamically and might degrade at elevated temperatures.

The (0 0 1) slabs of ReO_3, WO_3, WO_3/ReO_3, and ReO_3/WO_3 presented in Fig. 1 have different electronic structures. In Fig. 3 we present the sums of projected densities of states for the two top layers of each slab. WO_3(0 0 1) is clearly different than other slabs due to the bandgap of ca. 1.0 eV. The three other slabs are conductive and the values of DOS at the Fermi level increase from WO_3/ReO_3 through ReO_3/WO_3 to ReO_3. As we will see in Sections 3.2 and 3.3, the overall reactivity of slabs increases in the same sequence.

3.2. Hydrogen adsorption

In this work, we focus on hydrogen adsorption on the surface, not its diffusion into bulk. We first studied atomic hydrogen adsorption on the four surfaces. Three possible surface sites, i.e., the single bonded terminal O_{1C}, the bridging double bonded O_{2C}, and the penta-coordinated metal site Re_{5C} (or W_{5C}) are available for hydrogen adsorption. The optimized structures for the ReO_3(0 0 1) surface are shown in Fig. 4. The structural parameters and adsorption energies are summarized in Table 1.

The calculated adsorption energies of a hydrogen atom range from −7.9 kJ/mol at the W_{5C} site of WO_3(0 0 1) to −296.3 kJ/mol at the O_{1C} site of ReO_3(0 0 1). The oxygen sites (O_{1C} and O_{2C}) are energetically more favorable than the metal sites (Re_{5C} and W_{5C}) to adsorb a hydrogen atom due to formation of surface hydroxyl groups. Compared to the bridging O_{2C} site, the unsaturated terminal O_{1C} is more reactive. Indeed, the adsorption energies at the O_{1C} sites are higher than at the O_{2C} sites by about 60–100 kJ/mol, with an exception of WO_3(0 0 1), for which the adsorption energies are comparable, 266.8 and 265.1 kJ/mol, respectively. For the most stable hydrogen adsorption configuration (O_{1C} site), the hydrogen binding on the ReO_3(0 0 1) surface is the strongest and accounts to 296.3 kJ/mol. It drops to 266.8 kJ/mol for ReO_3/WO_3 illustrating the effect of the heterostructure. The atomic hydrogen adsorption at the M_{5C} site (M = W or Re) exposes differences between tungsten and rhenium. The adsorption at the W_{5C} site of WO_3(0 0 1) is very weak (−7.9 kJ/mol) with a W_{5C}–H bond distance of 2.34 Å, indicating a physisorbed bonding state. On the other hand, the

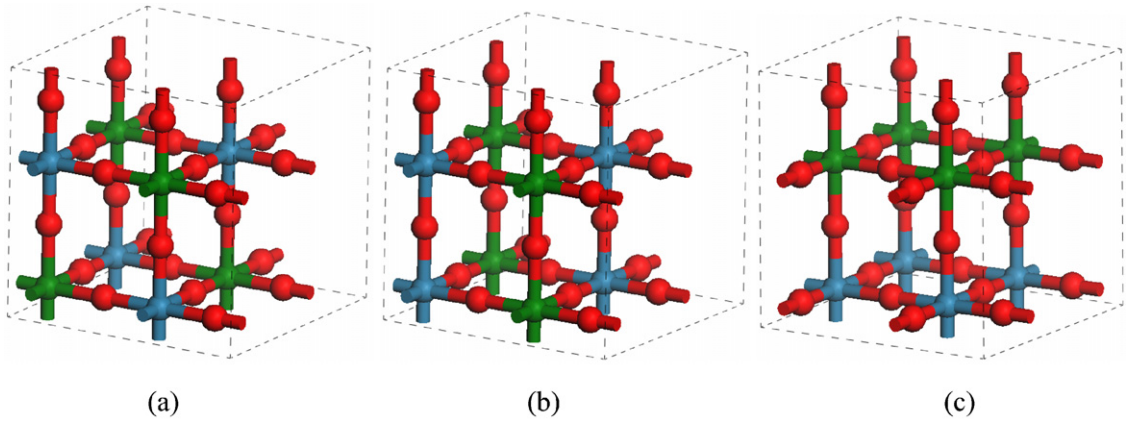

Fig. 2. Optimized geometries of three hypothetical bulk $WReO_6$ structures.

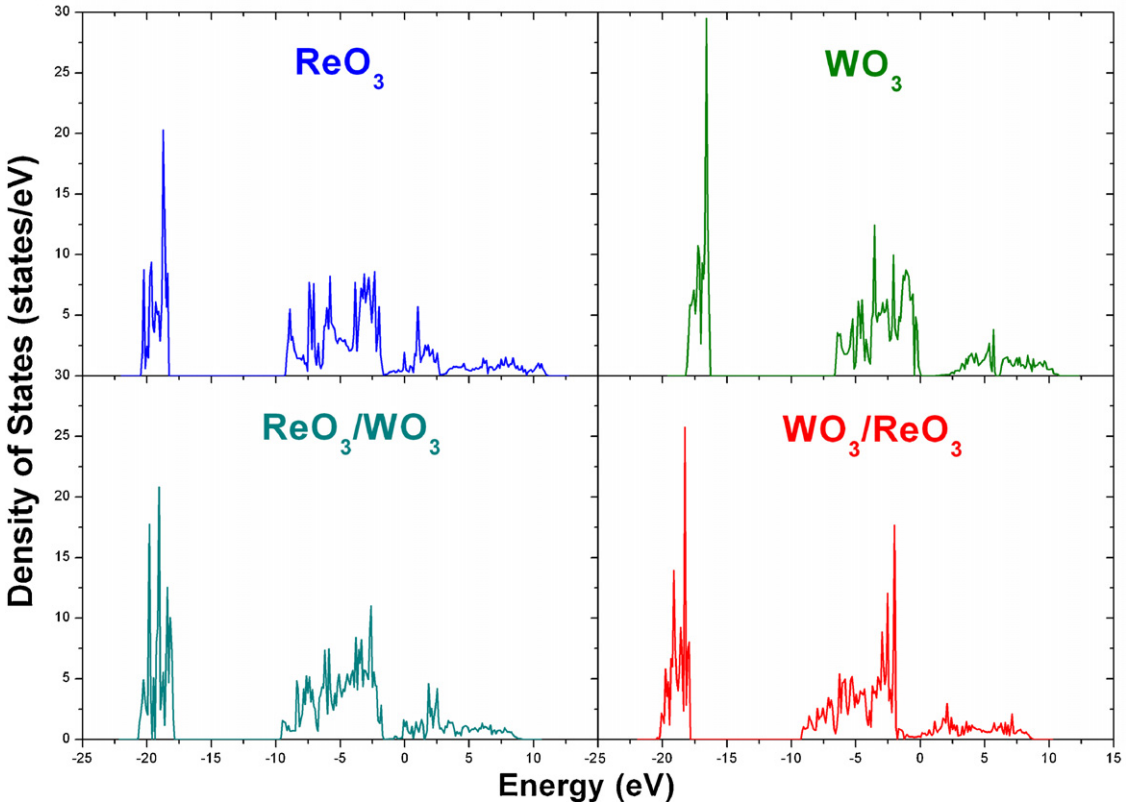

Fig. 3. Sums of projected DOS for the two top layers of the four surface slabs. The zero of energy is set to the Fermi level of each system.

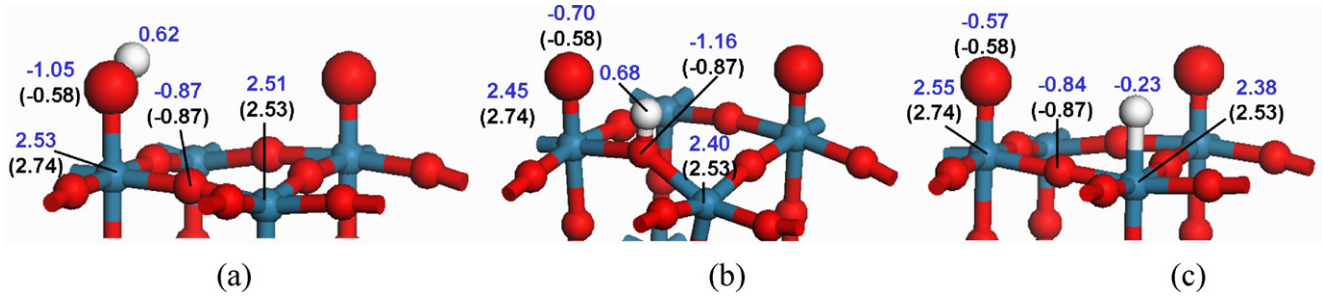

Fig. 4. Calculated Bader's charge changes upon atomic hydrogen adsorption on the ReO_3(0 0 1) surface: (a) H on O_{1C} site; (b) H on O_{2C} site; (c) H on Re_{5C} site. The numbers in black represent the charges before adsorption. The numbers in blue represent the charges after adsorption. (For interpretation of the references to color in this figure legend, the reader is referred to the web version of the article.)

Table 1
Energetics (kJ/mol) and structural parameters (Å) of atomic hydrogen adsorption on four model surfaces. The O_s represents the bonded surface oxygen atom. The subscript "s" indicates the site the hydrogen atom is bonded to, i.e., either O_s or M_s.

Surface	Adsorption site	E_{ad}	M_{6C}–O_{1C}	M_{6C}–O_{2C}	M_{5C}–O_{2C}	O_s–H/M_s–H
ReO_3	O_{1C}	−296.3	1.93	1.91	1.88	0.98
	O_{2C}	−200.1	1.76	2.08	2.04	0.98
	Re_{5C}	−141.5	1.72	1.91	1.87	1.71
WO_3	O_{1C}	−266.8	1.88	1.88	1.92	0.97
	O_{2C}	−265.1	1.71	2.06	2.04	1.00
	W_{5C}	−7.9	1.71	1.90	1.93	2.34
WO_3/ReO_3	O_{1C}	−278.3	1.88	1.92	1.88	0.96
	O_{2C}	−211.2	1.73	2.10	2.05	0.98
	W_{5C}	−48.9	1.71	1.92	1.89	1.73
ReO_3/WO_3	O_{1C}	−266.8	1.93	1.92	1.87	0.98
	O_{2C}	−207.3	1.73	2.05	2.04	1.00
	Re_{5C}	−152.3	1.71	1.88	1.88	1.72

adsorption energy at the Re_{5C} site of ReO_3(0 0 1) is −141.5 kJ/mol and the Re_{5C}–H bond length is much shorter, 1.71 Å. Overall, atomic hydrogen interacts with the conductive ReO_3(0 0 1) surface more strongly than with the insulating WO_3(0 0 1) surface. Perusal of the results for WO_3 and WO_3/ReO_3 further illustrates the effect of heterostructure. In comparison with WO_3, WO_3/ReO_3 offers a strong preference for adsorption at the O_{1C} site, and the adsorption energy at the W_{5C} site is increased to −48.9 kJ/mol. These differences must be attributed to the ReO_3 substrate.

To get more insights on how the variation of electronic structure affects the hydrogen adsorption, we performed Bader's charge analysis and projected density of states (PDOS) calculations. Fig. 4 shows the Bader's charges for the bare ReO_3(0 0 1) slab and for the same slab with a hydrogen atom adsorbed at the Re_{5C}, O_{1C}, and O_{2C} sites. For hydroxyl groups resulting from hydrogen adsorption at the O_{1C}, and O_{2C} sites, the effective charge on hydrogen is positive and effective negative charges on oxygen become more pronounced illustrating partial electron transfer from hydrogen to oxygen. On the other hand, a hydrogen atom adsorbed at the Re_{5C} site acquires an effective negative charge, an indication a partial electron transfer from rhenium to hydrogen. In consequence, a hydridic hydrogen is formed, though its adsorption energy is not competitive with the O_{1C} and O_{2C} sites. From PDOS plots shown in Fig. 5, it is clear that the antibonding 2p states of O_{1C} and O_{2C}, and antibonding 5d states of Re_{5C} atom are responsible for the hydrogen adsorption.

Different adsorption configurations were considered for molecular and dissociative adsorptions of a hydrogen molecule: (i) dissociative adsorption at the O_{2C} site; (ii) dissociative adsorption at neighboring O_{2C} sites; (iii) dissociative adsorption with one hydrogen atom at the O_{2C} site and another at the M_{5C} site; (iv) molecular hydrogen adsorption at the M_{5C} site; (v) dissociative adsorption at the O_{1C} site; (vi) dissociative adsorption at the O_{1C} and O_{2C} sites. Our results indicate that the adsorption energies are positive or larger than −3 kJ/mol for the first four cases. For this reason only the last two configurations are further considered and adsorption energies of a hydrogen molecule on the four surfaces are summarized in Table 2. A hydrogen molecule dissociatively adsorbed at the O_{1C} site can be viewed as a water molecule adsorbed at the M_{5C} site.

We will use a label "State 1" for a hydrogen molecule dissociatively adsorbed at the O_{1C} site and "State 2" for a hydrogen molecule dissociatively adsorbed at the O_{1C} site and at an adjacent O_{2C} site. The adsorption energies and energy barriers for the State 1 ↔ State 2 transformations are illustrated in Fig. 6. One might expect that the stability of the both dissociatively adsorbed states will be the largest for the metallic slab ReO_3 followed by the ReO_3/WO_3 heterostructure. In the latter, the topmost layer is the reactive ReO_3. However, the stability of State 1 evolves as $WO_3/ReO_3 > ReO_3 > ReO_3/WO_3 > WO_3$ illustrating unexpected properties of the WO_3/ReO_3 heterostructure. The stability of State 2 evolves as $ReO_3 > WO_3/ReO_3 > ReO_3/WO_3 > WO_3$ illustrating again unexpected properties of the WO_3/ReO_3 heterostructure. State 1 is energetically more favorable than State 2 for all slabs, with the relative stability exceeding 32 kJ/mol for WO_3/ReO_3 and ReO_3 and being smaller than 18 kJ/mol for WO_3 and ReO_3/WO_3.

State 1 and State 2 might interconvert between each other. Thus we considered energetic barriers for the State 1 ↔ State 2 transformations. The forward reaction would correspond to breaking an O_{1C}–H bond from State 1 and transferring the hydrogen atom to a nearby O_{2C} atom. The results of NEB calculations for transition states (TS1-2) are summarized in Fig. 6 and geometries of transition states are summarized in Table 2. The energies in Fig. 6 are referenced with respect to State 0, which represents a bare slab and an isolated hydrogen molecule. As discussed above, the State 1 → State 2 reaction is endothermic for all slabs and the barrier for the forward reaction is the smallest for the ReO_3/WO_3 slab (49.1 kJ/mol) and the largest for the WO_3 slab (70.9 kJ/mol). For the reverse reaction the smallest barrier is for the WO_3/ReO_3 slab (23.6 kJ/mol) and the largest for the WO_3 slab (53.5 kJ/mol).

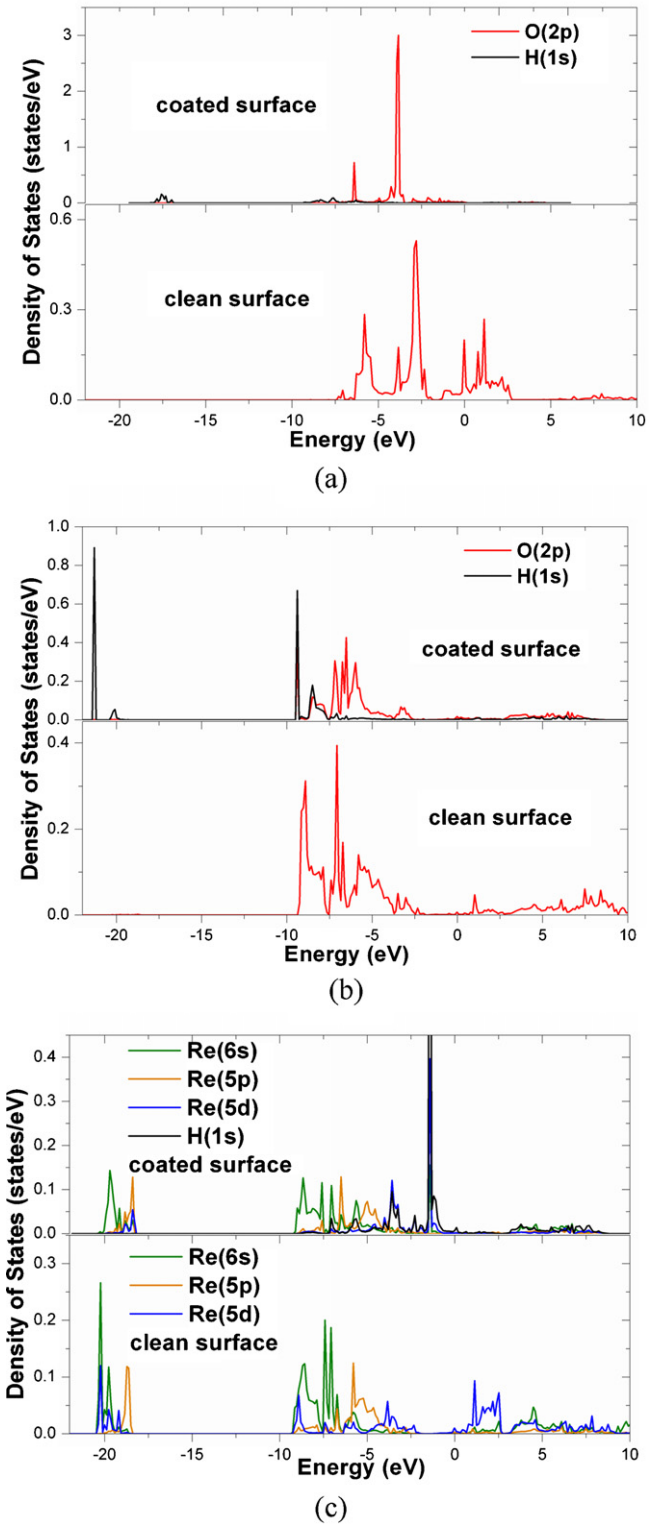

Fig. 5. DOS plots upon atomic hydrogen adsorption on the ReO_3(0 0 1) surface: (a) H on O_{1C} site; (b) H on O_{2C} site; (c) H on Re_{5C} site. The zero of energy is set to the Fermi level of each system.

Table 2
Energetics (kJ/mol) and structural parameters (Å) of dissociative adsorption of hydrogen molecule on four model surfaces.

Surface	Adsorption sites	E_{ad}	M_{6C}–O_{1C}	M_{6C}–O_{2C}	M_{5C}–O_{2C}	O_{1C}–H	$O_{1C}\cdots H(O_{2C})$
ReO_3	$O_{1C}+O_{1C}$	−100.3	2.23	1.90	1.89	0.98	
	$O_{1C}+O_{2C}$	−68.2	1.98	2.05	2.05	0.97	2.07
	TS		2.09	2.03	1.98	0.97	1.33
WO_3	$O_{1C}+O_{1C}$	−46.7	2.32	1.90	1.91	0.98	
	$O_{1C}+O_{2C}$	−29.3	1.89	2.06	2.03	0.97	3.16
	TS		2.08	2.07	1.96	0.97	1.37
WO_3/ReO_3	$O_{1C}+O_{1C}$	−113.6	2.33	1.93	1.92	0.98	
	$O_{1C}+O_{2C}$	−67.1	1.94	2.10	2.04	0.97	2.90
	TS		1.97	2.09	2.04	0.97	2.19
ReO_3/WO_3	$O_{1C}+O_{1C}$	−58.8	2.21	1.94	1.91	0.98	
	$O_{1C}+O_{2C}$	−50.3	1.94	2.10	2.05	0.98	3.16
	TS		2.08	2.03	1.99	0.97	1.36

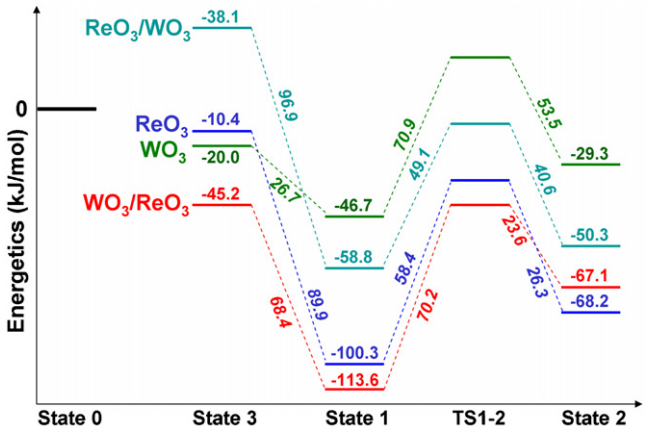

Fig. 6. Adsorption energies and barrier heights for molecular hydrogen on four model surfaces. Values of reaction barriers are italicized.

Taking ReO_3 as an example, we show the optimized structures of State 1, TS1-2 and State 2 in Fig. 7. This figure and geometries listed in Table 2 illustrate that the slab is only slightly distorted in State 1. As hydrogen transfers through TS1-2 to State 2 a significant geometry relaxation of the slab is observed. In the initial state, which resembles a water molecule adsorbed at the R_{5C} site, the O_{1C}–H distance is only 0.97 Å. Next, the H(O_{1C}) atom approaches the O_{2C} atom and the O_{1C}–H distance increases to 1.33 Å at TS1-2. This structural rearrangement is accompanied by a pronounced surface relaxation. In the final state, one hydrogen atom is bound at the O_{2C} site and its distance from the O_{1C} site becomes 2.07 Å. The surface remains strongly distorted upon formation of the O_{1C}–H and O_{2C}–H hydroxyl groups. Similar surface relaxation was observed for the State 1 → State 2 reaction on three other slabs.

One might expect that the conductive ReO_3 surface will be the most favorable for the State 1 → State 2 reaction. The calculated barrier is, however, significant, 58.4 kJ/mol, and the reaction is endothermic by 32.1 kJ/mol. A significant improvement is observed for the ReO_3/WO_3 slab, for which the barrier is reduced to 49.1 kJ/mol and the endothermicity to 8.4 kJ/mol! Thus the heterostructure ReO_3/WO_3 displays better properties for dissociation of molecular hydrogen than the ReO_3 surface. Perusal of Fig. 6 also illustrates activation of the WO_3 surface by putting the ReO_3 monolayer on the top and "passivation" of the ReO_3 surface by putting the WO_3 monolayer on the top.

Next we analyze the State 2 → State 1 reaction, which is equivalent to recombination of the O_{1C}–H and O_{2C}–H hydroxyl groups and formation of a water molecules (H_2O_{1C}) adsorbed on the surface metal site. The reaction is exothermic for all four slabs, in particular for WO_3/ReO_3 (−46.5 kJ/mol) and ReO_3 (−32.1 kJ/mol). The same two slabs offer the lowest barriers for the recombination step: 23.6 kJ/mol for WO_3/ReO_3 and 26.3 kJ/mol for ReO_3, see Fig. 6. These barriers are much lower than the corresponding barriers (53.5 and 40.6 kJ/mol) on the WO_3 and ReO_3/WO_3 surfaces. Advantageous properties of WO_3/ReO_3 in comparison with ReO_3 illustrate that epitaxial heterostructures might be useful in catalytic applications. Similarly, the reactivity of WO_3(0 0 1) can be improved by adding an overlayer of ReO_3.

In addition to State 1 and State 2, we also consider State 3 (see Fig. 6), which results from a water molecule desorption from the surface and formation of a partially reduced (0 0 1) surface. We find that on the WO_3 surface, the State 1 → State 3 reaction is endothermic by 26.7 kJ/mol, and the stabilities of State 2 and State 3 are comparable, with State 3 being more stable by only 9.4 kJ/mol. The results presented above are consistent with experimental findings, which indicated that adsorption of hydrogen on WO_3 could lead to metallic tungsten via formation of hydroxyl groups and desorption of water [17]. Another interesting finding is that State 3 is less stable

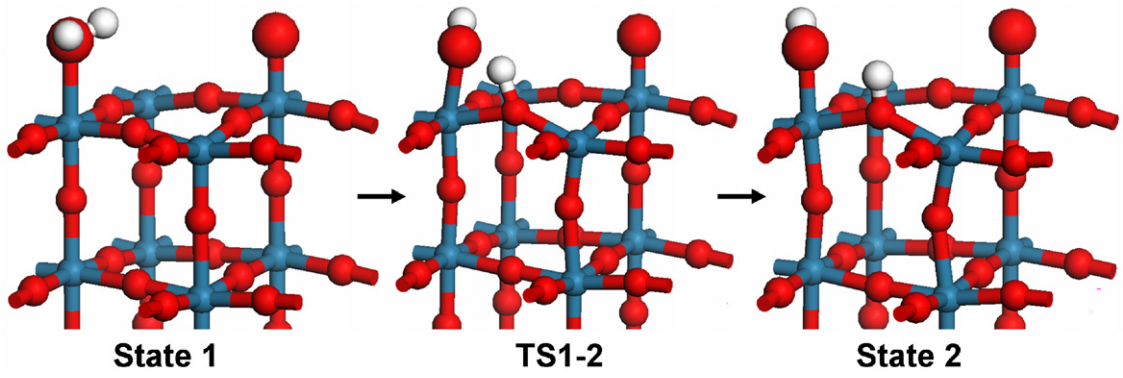

Fig. 7. Sideview of optimized geometries of different surface states for adsorption of a hydrogen molecule on the pure ReO_3(0 0 1) surface.

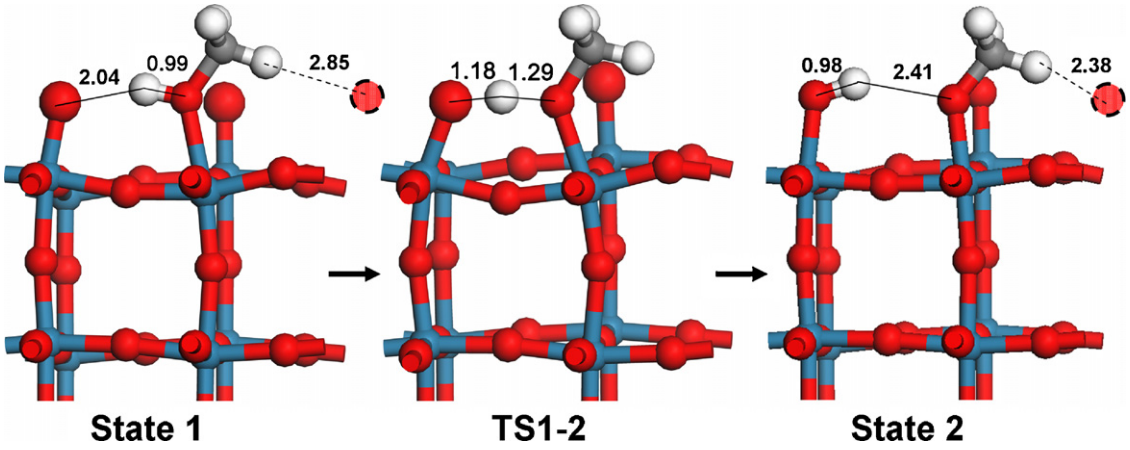

Fig. 8. Methanol dissociation path on the ReO_3(0 0 1) surface.

than State 0 for the ReO_3/WO_3 surface by 38.1 kJ/mol. It implies that water molecules would not only adsorb on the reduced ReO_3/WO_3 surface but they could also release molecular hydrogen.

3.3. Methanol molecular adsorption and dissociation

Methanol can molecularly adsorb at the M_{5C} site (State 1) and dissociatively adsorb at the O_{1C} and M_{5C} sites (State 2). As shown in Fig. 8 for ReO_3(0 0 1), methanol molecularly adsorbs via the O–M_{5C} bonding. The calculated adsorption energy spans a range from 65.6 kJ/mol for WO_3 to 95.3 kJ/mol for ReO_3, see Fig. 9 and Table 3. The adsorption energies roughly correlate with the M_{5C}–O(OH) distance, which is the shortest for ReO_3 and the longest for WO_3. These distances are significantly longer than the M_{5C}–O_{2C} distances and illustrate the physisorbed state of methanol. The calculated methanol adsorption energy on WO_3 is −65.6 kJ/mol. This is in good agreement with previous experimental estimation of −67 kJ/mol [4].

We considered dissociation of molecularly adsorbed methanol via O–H bond breaking into a methoxy group and formation of a surface hydroxyl HO_{1C}. As discussed in Section 1, different decomposition paths were observed on the pure ReO_3 and WO_3 surfaces. Supported ReO_3 was found to be catalytically very active [6,14] while WO_3 is practically inactive for methanol dissociation under UHV conditions [4]. We first examined methanol dissociation on WO_3(0 0 1). We found that methanol dissociation is highly endothermic with a reaction energy of +102.5 kJ/mol, see also Ref. [18]. This is consistent with experimental findings [4] that methanol does not dissociate on the WO_3(0 0 1) surface. We further calculated methanol dissociation on other three slabs.

The stability of State 2 decreases from ReO_3 through ReO_3/WO_3 to WO_3/ReO_3 and the adsorption energies span a broad range from

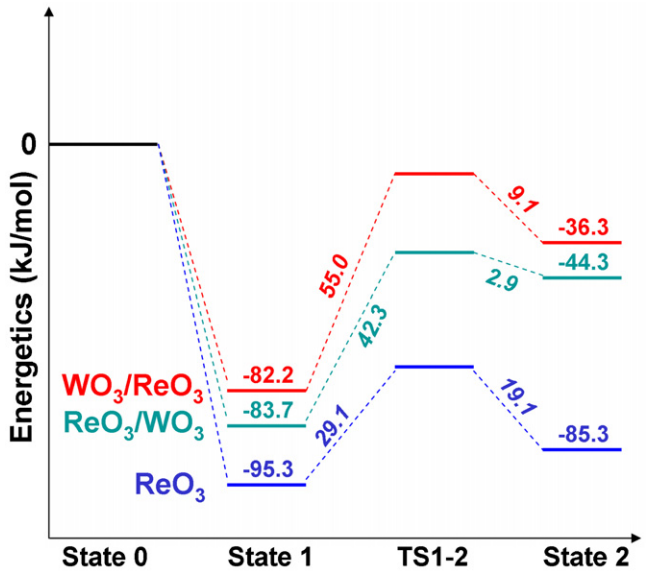

Fig. 9. Adsorption energies and barrier heights for methanol on selected model surfaces. Values of reaction barriers are italicized.

−85.3 to −36.3 kJ/mol. The State 1 → State 2 reaction is endothermic for all four slabs, see Table 3 and Fig. 9. We also note that the endothermicity of methanol dissociation is surface dependent. For example, methanol dissociation on the ReO_3(0 0 1) surface (shown in Fig. 8) is slightly endothermic (+10 kJ/mol). The endothermicity increases to 39.3 kJ/mol for ReO_3/WO_3 and 45.9 kJ/mol for WO_3/ReO_3. This trend is maintained for the forward barriers, with the smallest for ReO_3 (29.1 kJ/mol) and the largest for WO_3/ReO_3

Table 3
Energetics (kJ/mol) and structural parameters (Å) of molecular and dissociative adsorptions of methanol on four model surfaces. The O(OH) and H(OH) denote the oxygen and hydrogen atom in the hydroxyl group of methanol, respectively. M denotes Re or W.

Surface	Adsorption mode	E_{ad}	M_{6C}–O_{1C}	M_{6C}–O_{2C}	M_{5C}–O_{2C}	M_{5C}–O(OH)	$O_{1C}\cdots$H(OH)	O(M)$\cdots$H(OH)
ReO_3	Molecular	−95.3	1.76	1.93	1.87	2.24	2.04	0.99
	Dissociative	−85.3	1.94	1.88	1.88	1.94	0.98	2.41
	TS		1.85	1.94	1.87	2.08	1.18	1.29
WO_3	Molecular	−65.6	1.73	1.92	1.88	2.38	2.17	0.98
	Dissociative	36.9	1.89	1.83	1.96	1.95	0.98	3.09
WO_3/ReO_3	Molecular	−82.2	1.74	1.95	1.87	2.29	2.07	0.98
	Dissociative	−36.3	1.88	2.06	1.79	1.98	1.02	1.69
	TS		1.87	2.04	1.79	2.00	1.03	1.65
ReO_3/WO_3	Molecular	−83.7	1.76	1.88	1.88	2.32	2.01	0.99
	Dissociative	−44.3	1.91	1.86	1.89	2.00	1.00	1.93
	TS		1.86	1.87	1.90	2.08	1.10	1.41

(55.0 kJ/mol). The small endothermicity and a low forward barrier for ReO_3 is in agreement with previous experimental finding [6,14] that the supported ReO_3 is a good catalyst for methanol decomposition reaction. We emphasize that the passive WO_3 surface is activated when engaged in the WO_3/ReO_3 and ReO_3/WO_3 heterostructures.

4. Summary

To understand surface reactivity of epitaxial heterostructures made of metal oxides displaying different electronic structure, a comparative study on adsorption and reactivity of hydrogen and methanol on model (0 0 1) surfaces of ReO_3, WO_3, as well as their heterostructures ReO_3/WO_3 and WO_3/ReO_3 has been performed at the density functional theory level. The wide bandgap WO_3 and the conductive ReO_3 have commensurate lattice constants and therefore can form heterostructures.

Atomic hydrogen adsorption at the terminal O_{1C} site is energetically most favorable on all four surfaces. The Bader's charge and PDOS analyses clearly suggest that the antibonding $O_{1C}(2p)$ is responsible for hydrogen adsorption.

Dissociative adsorption of a hydrogen molecule at the O_{1C} site leads to formation of a water molecule adsorbed at the surface M_{5C} site. This is thermodynamically the most stable state. A thermodynamically less stable dissociative state involves two surface hydroxyl groups $O_{1C}H$ and $O_{2C}H$. We also determined energy barriers that separate these two states. The interaction of hydrogen with pure ReO_3 is stronger than with pure WO_3 and the strength of the interaction substantially changes for the WO_3/ReO_3 and ReO_3/WO_3 heterostructures. In particular, the barrier and endothermicity for the forward reaction are reduced by 9.3 and 23.7 kJ/mol upon the replacement of ReO_3 with ReO_3/WO_3. The recombination of the O_{1C}–H and O_{2C}–H hydroxyl groups and formation of a water molecules (H_2O_{1C}) adsorbed on the surface metal site was found to be exothermic for all four slabs, in particular for WO_3/ReO_3 (−46.5 kJ/mol) and ReO_3 (−32.1 kJ/mol). The same two slabs offer the lowest barriers for the recombination step: 23.6 kJ/mol for WO_3/ReO_3 and 26.3 kJ/mol for ReO_3.

We considered dissociation of molecularly adsorbed methanol via O–H bond breaking into a methoxy group and formation of a surface hydroxyl HO_{1C}. In agreement with past experimental observations, our calculations show that methanol does not dissociate on WO_3(0 0 1), with the dissociation barrier exceeding 100 kJ/mol. The calculated adsorption energy of methanol on WO_3(0 0 1) of −65.6 kJ/mol is consistent with the previous experimental estimation of −67 kJ/mol. However, the reactivity of methanol increases on the ReO_3/WO_3 and WO_3/ReO_3 heterostructures, with the ReO_3 surface remaining the most reactive. This work demonstrates that reactivity of metal oxides can be tuned by making epitaxial heterostructures.

Acknowledgments

We thank Prof. Q. Ge (Southern Illinois University) for helpful discussions. We thank Prof. B. Frederick (University of Maine) for providing updated experimental estimation of the adsorption energy of methanol on the oxidized WO_3(0 0 1) surface. S.L. and M.G. thank PNNL for providing a fellowship through the Summer Research Institute program. D.M. is supported by a LDRD project from Catalysis Initiative at PNNL. The computing time was granted by the National Energy Research Scientific Computing (NERSC) Center at Lawrence Berkeley National Laboratory and the computational catalyst design project (gc34000) at the William R. Wiley Environmental Molecular Sciences Laboratory (EMSL). EMSL is a DOE national scientific user facility located at PNNL.

References

[1] V.E. Henrich, P.A. Cox, The Surface Science of Metal Oxides, Cambridge University Press, Cambridge, 1994.
[2] A.S.Y. Chan, W. Chen, H. Wang, J.E. Rowe, T.E. Madey, J. Phys. Chem. B 108 (2004) 14643.
[3] F. Cora, M.G. Stachiotti, C.R.A. Catlow, C.O. Rodriguez, J. Phys. Chem. B 101 (1997) 3945.
[4] S. Ma, F.G. Amar, B.G. Frederick, J. Phys. Chem. A 107 (2003) 1413.
[5] S. Ma, B.G. Frederick, J. Phys. Chem. B 107 (2003) 11960.
[6] Y.H. Yuan, Y. Iwasawa, J. Phys. Chem. B 106 (2002) 4441.
[7] S.A. Chambers, J. Phys.: Condens. Matter 20 (2008) 264004.
[8] S.A. Chambers, Y. Liang, Y. Gao, Phys. Rev. B 61 (2000) 13223.
[9] J.E. Jaffe, M. Dupuis, M. Gutowski, Phys. Rev. B 69 (2004) 205106.
[10] J.E. Jaffe, R.A. Bachorz, M. Gutowski, Phys. Rev. B 75 (2007) 205323.
[11] M.A. Butler, R.D. Nasby, R.K. Quinn, Solid State Commun. 19 (1976) 1011.
[12] M. Li, W. Gao, A. Posadas, C.H. Ahn, E.I. Altman, J. Phys. Chem. B 108 (2004) 15259.
[13] R.E. Tanner, P. Meethunkij, E.I. Altman, J. Phys. Chem. B 104 (2000) 12315.
[14] Y. Yuan, T. Shido, Y. Iwasawa, Chem. Commun. (2000) 1421.
[15] A.R. Berzins, P.A. Sermon, Nature 303 (1983) 506.
[16] S. Horiuchi, N. Kimizuka, A. Yamamoto, Nature 279 (1979) 226.
[17] R.D. Bringans, H. Hochst, H.R. Shanks, Surf. Sci. 111 (1981) 80.
[18] I.N. Yakovkin, M. Gutowski, Surf. Sci. 601 (2007) 1481;
I.N. Yakovkin, M. Gutowski, Unpublished results.
[19] Q. Ge, M. Gutowski, Unpublished results.
[20] P.M. Woodward, A.W. Sleight, T. Vogt, J. Solid State Chem. 131 (1997) 9.
[21] J.E. Schirber, B. Morosin, Phys. Rev. Lett. 42 (1979) 1485.
[22] G. Kresse, J. Hafner, Phys. Rev. B 47 (1993) 558.
[23] G. Kresse, J. Furthmuller, Comput. Mater. Sci. 6 (1996) 15.
[24] J.P. Perdew, K. Burke, M. Ernzerhof, Phys. Rev. Lett. 77 (1996) 3865.
[25] P.E. Blochl, Phys. Rev. B 50 (1994) 17953.
[26] D. Hobbs, G. Kresse, J. Hafner, Phys. Rev. B 62 (2000) 11556.
[27] H.J. Monkhorst, J.D. Pack, Phys. Rev. B 13 (1976) 5188.
[28] R.F.W. Bader, Acc. Chem. Res. 18 (1985) 9.
[29] G. Henkelman, A. Arnaldsson, H. Jonsson, Comput. Mater. Sci. 36 (2006) 354.
[30] G. Henkelman, B.P. Uberuaga, H. Jonsson, J. Chem. Phys. 113 (2000) 9901.